引用格式：PAN Wanle, CHEN Heming, HU Yuchen. Three-channel Integrated Device for Graphene Electro-optic Modulation and Mode Division Multiplexing[J]. Acta Photonica Sinica, 2023, 52(2):0213001
潘万乐,陈鹤鸣,胡宇宸. 三信道石墨烯电光调制和模分复用集成器件[J].光子学报,2023,52(2):0213001

三信道石墨烯电光调制和模分复用集成器件

潘万乐[1],陈鹤鸣[2],胡宇宸[1]
(1 南京邮电大学 电子与光学工程学院,南京 210023)
(2 南京邮电大学 贝尔英才学院,南京 210023)

摘 要:提出了一种三信道石墨烯电光调制和模分复用集成器件,该器件由单层石墨烯覆盖的一维光子晶体纳米梁腔电光调制模块和纳米线波导模分复用模块组成。利用三维时域有限差分法进行仿真分析,结果表明,该器件可以同时实现TE_0模、TE_1模和TE_2模的调制和模分复用功能。当波长为1 570 nm时,消光比大于28.3 dB,插入损耗小于0.21 dB,信道串扰小于−28.6 dB,调制器的3 dB带宽达到100 GHz,器件尺寸约为100 μm×13 μm。该集成器件性能优良,在大容量光通信系统中具有重要的应用价值。

关键词:石墨烯;纳米线波导;电光调制;模分复用;硅基光电子集成
中图分类号:TN256 **文献标识码**:A **doi**:10.3788/gzxb20235202.0213001

0 引言

互联网时代,光通信系统对于传输速度和传输容量的需求越来越高。用于光通信系统的电光调制器向着高速度方向发展。传统硅基电光调制器,响应速度较慢[1-2]。石墨烯具有优异的光电特性,并且与互补金属氧化物半导体(Complementary Metal Oxide Semiconductor, CMOS)工艺兼容,将石墨烯与硅材料结合,可以提高电光调制器的响应速度[3]。宽带宽、高消光比、低插入损耗、低能耗是石墨烯电光调制器的发展趋势[4-8]。另一方面,为了满足光通信的需要,模分复用(Mode Division Multiplexing, MDM)等复用技术用来增加通信容量,模分复用器是模分复用的关键器件。各种不同类型的模分复用器件被广泛研究,比如Y结型[9]、微环谐振腔型[10]、绝热耦合型[11]、微盘谐振腔型[12]。

随着科技不断进步,光互联因其高速度、宽带宽、大容量的优点得到广泛关注,各种集成器件应运而生[13-16]。JIA H等[17]提出了一种用于片上光互连的模式选择调制器,该器件采用硅微环谐振腔和非对称定向耦合器结构,可以实现TE_0、TE_1、TE_2、TE_3模的调制和模分复用功能,插入损耗小于2.1 dB,信道串扰小于−19.7 dB。WU X R等[18]提出了一种应用于模分复用系统的硅微环调制器,利用三个不同的微环调制器进行调制,然后通过模分复用器,三束信号光以TE_0、TE_1和TE_2模的形式复用到多模波导,在波长1 551.523 nm处,信道串扰小于−23.1 dB,调制器的3 dB带宽约为17 GHz,但是该器件的插入损耗大于10 dB。CHEN G Y等[19]提出了一种片上模分复用光子互连系统,在调制和模分复用过程中均采用微环谐振腔结构,该器件的消光比大于36.5 dB,信道串扰小于−30 dB,插入损耗小于4.1 dB,在3 V的电压下,3 dB带宽仅为36 GHz左右。

本文提出一种三信道石墨烯电光调制和纳米线波导模分复用集成器件,该器件由单层石墨烯覆盖的一维光子晶体纳米梁腔电光调制模块和纳米线波导模分复用模块组成。利用三维时域有限差分法(Three-Dimensional Finite-Difference Time-Domain, 3D-FDTD)进行仿真分析。结果表明,该器件可以同时实现TE_0模、TE_1模和TE_2模的调制和模分复用功能,且器件尺寸较小、消光比高、信道串扰小、插入损耗低、带宽

基金项目:国家自然科学基金(No. 61571237),江苏省自然科学基金(No. BK20151509),江苏省研究生科研与实践创新计划项目(Nos. KYCX20_0740, KYCX20_0769)
第一作者:潘万乐,1018020902@njupt.edu.cn
通讯作者:陈鹤鸣,chhm@njupt.edu.cn
收稿日期:2022-09-22;**录用日期**:2022-11-10

大,性能优良。

1 理论模型和工作原理

1.1 理论模型

电光调制器的理论模型如图1所示,该模型采用谐振腔与波导侧耦合结构。在图1中,S_{+1}和S_{+2}表示输入波幅值,S_{-1}和S_{-2}表示输出波幅值,γ_1和γ_2表示衰减系数。在调制器的"断"状态下,即入射光全部反射回入射端口。假设谐振腔的谐振频率为ω_0,谐振腔的谐振模振幅为a。令$\gamma_1=\gamma_2=\gamma$,其时域耦合模方程如下。

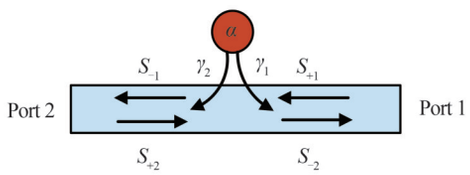

图1 电光调制器的理论模型

Fig. 1 Theoretical model of electro-optic modulator

谐振腔的谐振模振幅的时域变化可以表示为[20]

$$\frac{\mathrm{d}a}{\mathrm{d}t}=-\mathrm{i}\omega_0 a-2\gamma a+\sqrt{2\gamma}\,(S_{+1}+S_{+2}) \tag{1}$$

由于输入光的谐振频率ω不变,即$a(t)=\exp(-\mathrm{i}\omega t)$,所以$\mathrm{d}a/\mathrm{d}t=-\mathrm{i}\omega a$[21]。当输入光只有$S_{+1}$($S_{+2}=0$)时,可得

$$a=\frac{\sqrt{2\gamma}}{\mathrm{i}(\omega_0-\omega)+2\gamma}\cdot S_{+1} \tag{2}$$

输入波和输出波幅值之间的关系为

$$S_{-1}=S_{+1}-\sqrt{2\gamma}\,a \tag{3}$$

于是得到端口2的下行效率$D(\omega)$为

$$D(\omega)=\left|\frac{S_{-1}}{S_{+1}}\right|^2=\left|\frac{\mathrm{i}(\omega_0-\omega)}{\mathrm{i}(\omega_0-\omega)+2\gamma}\right|^2 \tag{4}$$

同理可以计算端口1的反射效率$R(\omega)$。

$$S_{-2}=S_{+2}-\sqrt{2\gamma}\,a \tag{5}$$

$$R(\omega)=\left|\frac{S_{-2}}{S_{+1}}\right|^2=\left|\frac{2\gamma}{\mathrm{i}(\omega_0-\omega)+2\gamma}\right|^2 \tag{6}$$

图2为端口1和端口2的理论透射谱图。当$\omega=\omega_0$时,下行效率为0,而反射效率为100%。也就是谐

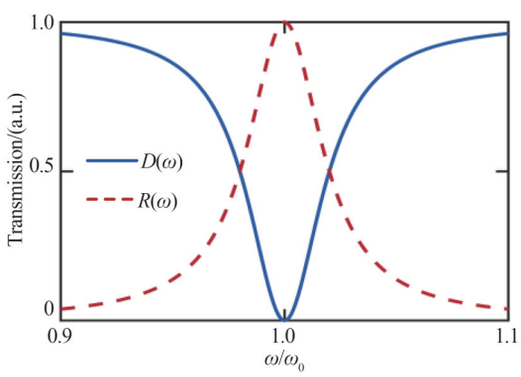

图2 理论模型透射谱

Fig. 2 Transmission spectrum of the theoretical model

振频率为ω的入射光被谐振腔全部反射回入射端口，调制器处于“断”状态。

1.2 工作原理

电光调制和模分复用集成器件的工作原理如图3所示，A_0、A_1和A_2是三个石墨烯电光调制器模块，B是纳米线波导MDM模块。在A_0模块中，波长为λ的TE_0模从右侧端口输入。当加上一定的驱动电压，使入射光的谐振波长与微腔的谐振波长相同，入射光被局域在微腔中，不能继续传输，实现调制器的“断”状态；当无外加电压时，入射光不与微腔耦合，可以沿着波导传输，实现调制器的“通”状态。A_1和A_2模块的工作原理与A_0模块相同。调制后的入射光分别进入MDM模块的三个端口，A_0模块的入射光进入多模波导，经过相位匹配区1和相位匹配区2光波不会发生模式转换，仍以TE_0模的形式从左侧端口输出。在相位匹配区1，A_1模块的入射光由TE_0模转换为TE_1模，并耦合至多模波导以TE_1模的形式从左侧端口输出。在相位匹配区2，A_2模块的入射光由TE_0模转换为TE_2模，并耦合至多模波导以TE_2模的形式从左侧端口输出。这样，从三个端口输入的TE_0模在MDM模块的同一端口输出，实现了调制和模分复用的功能。

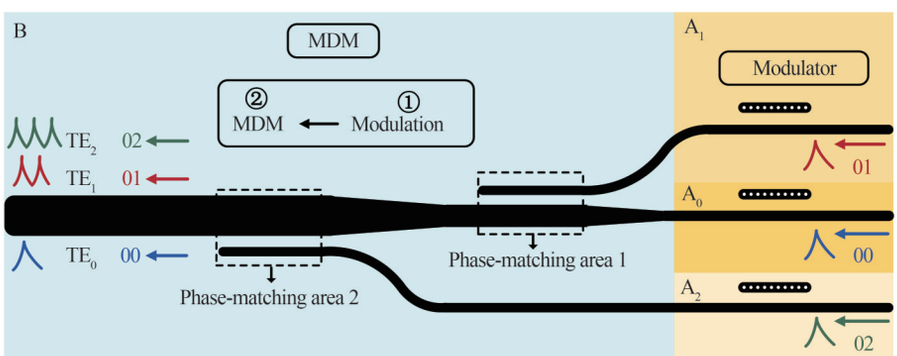

图3 电光调制和模分复用集成器件的工作原理

Fig. 3 Working principle of electro-optic modulation and MDM integrated device

2 结构设计与性能分析

三信道石墨烯电光调制和纳米线波导模分复用集成器件的三维结构如图4所示。该结构衬底为硅（折射率3.47），厚度约为2.5 μm；包层为二氧化硅（折射率1.44），厚度约为3 μm，由单层石墨烯覆盖的一维光子晶体纳米梁腔电光调制模块和纳米线波导模分复用模块组成。以下分别对石墨烯电光调制器和纳米线波导模分复用器进行单独的结构设计。

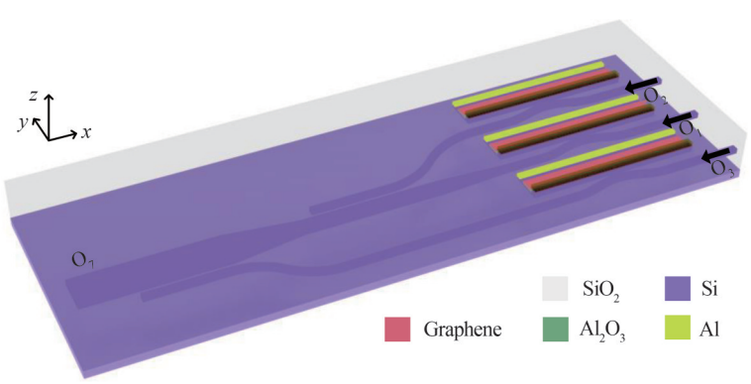

图4 电光调制和模分复用集成器件的三维结构图

Fig. 4 Three-dimensional schematic diagram of electro-optic modulation and MDM integrated device

2.1 石墨烯电光调制器的结构设计

本文提出的石墨烯电光调制器，其三维结构如图5(a)所示。该调制器采用纳米线波导与一维光子晶体纳米梁腔侧耦合结构。微腔中间位置处，纳米线波导采用弯曲波导结构，微腔与波导的间距为g_1=210 nm，可以实现微腔与波导的高效耦合；微腔两端部分，纳米线波导采用直波导结构，微腔与波导的间距为g_2=

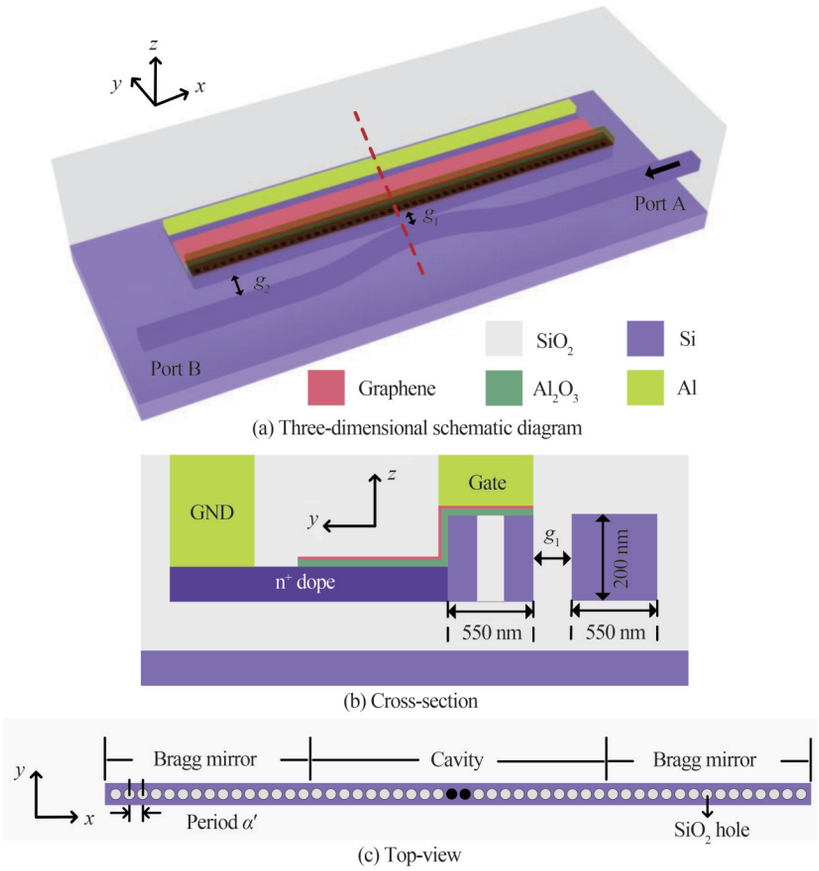

图 5 电光调制器结构

Fig. 5 Structural diagrams of electro-optic modulator

560 nm。

图 5(a)微腔中心位置红色虚线处剖面的三维结构侧视图如图 5(b)所示，纳米线波导和一维光子晶体纳米梁腔的宽度均为 550 nm，厚度为 200 nm。纳米梁腔左侧是厚度为 15 nm 的硅板，相当于调制器的 n 型掺杂区域。在硅板的部分区域和微腔顶部覆盖一层 Al_2O_3，厚度为 7 nm。单层石墨烯材料添加在 Al_2O_3 顶部。石墨烯上的电极作为阳极，硅板上的电极作为阴极。

一维光子晶体纳米梁腔的二维平面图如图 5(c)所示。所有的圆孔沿 x 轴方向排列，晶格常数为 $a'=350$ nm。圆孔内用二氧化硅填充。微腔两侧表示的是布拉格反射镜，圆孔的半径为 $r_1=103$ nm；中间表示的是光子晶体微腔区域，圆孔的半径由两侧的 105 nm 增加至中间的 114 nm。微腔中间两个圆孔(黑色标记)的半径为 $r_2=112$ nm，目的是使得微腔的谐振波长与目标波长(1 570 nm)失配，实现调制器的“通”状态。

材料的等效折射率 n_{eff} 随电压的变化如图 6(a)所示。随着电压的增大，Δn_{eff} 不断增大。当电压为 8 V 时，Δn_{eff} 最大变化为 0.005 5，比传统光学调制器 Δn_{eff} 高一个数量级[22-23]。利用 Lumerical 对该调制器进行 3D-FDTD 仿真。将宽光谱的 TE_0 模光源放置在端口 A，在端口 B 放置探测器，得到不同电压下的透射谱如图 6(b)所示。在 1 570 nm 波长下，当电压 $U=0$ V 时，透过率为 98.5%，调制器为“通”状态；当电压 $U=3.8$ V 时，透过率为 0.56%，调制器为“断”状态，此时材料等效折射率的变化为 0.002 3。插入损耗为 0.07 dB，消光比为 22.5 dB。

调制器的 3 dB 带宽是衡量调制器性能优劣的重要参数，其公式表示为

$$f_{3\,\mathrm{dB}}=\frac{1}{2\pi RC} \tag{7}$$

式中，R 为器件的电阻，大小约为 20 Ω[24]。C 为石墨烯的电容，可以表示为

$$C=\frac{\varepsilon_0\varepsilon_d A}{d} \tag{8}$$

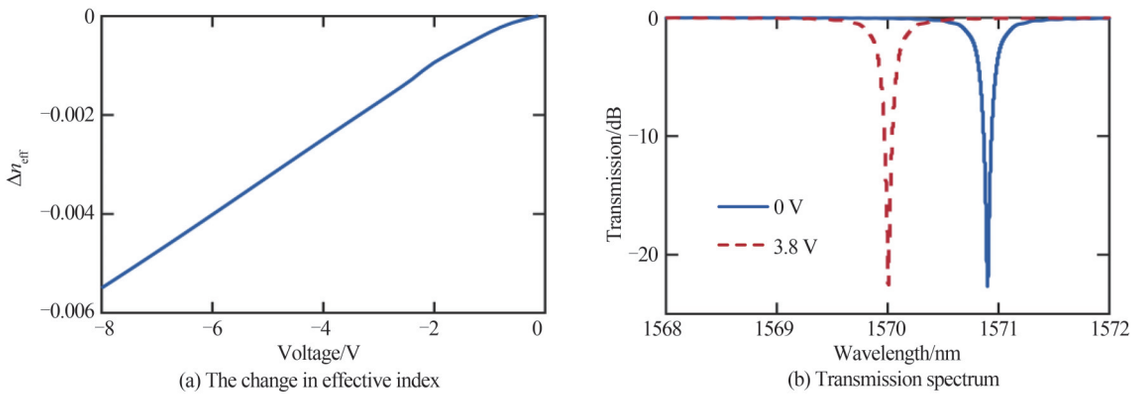

图 6　等效折射率的变化和透射谱

Fig. 6　The change in effective index and transmission spectrum

式中，ε_0为真空介电常数；ε_d为Al_2O_3的相对介电常数，ε_d＝9.34；A为单层石墨烯的面积，约为6 μm^2；d为Al_2O_3的厚度，d=7 nm。代入式(8)可以计算出电容C约为70 fF。最后，得到调制器的3 dB带宽约为114 GHz。调制器的能耗($E=C\cdot U^2/4$)[5]约为0.25 pJ/bit。利用Lumerical仿真得到调制器的3 dB带宽如图7所示，其大小约为100 GHz。计算得到的3 dB带宽与仿真相比有一定误差，主要原因是器件的电阻R为估计值，导致计算结果有一定偏差。

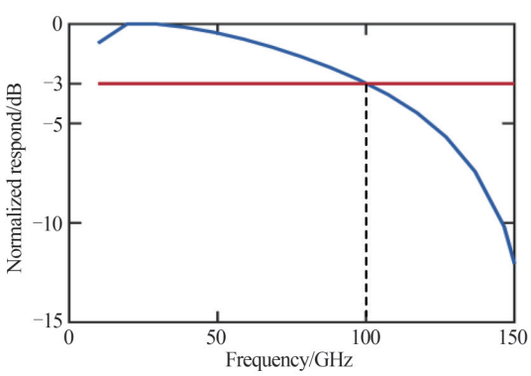

图 7　调制器的3 dB带宽

Fig. 7　3 dB bandwidth of the modulator

利用Lumerical对石墨烯电光调制器进行3D-FDTD仿真，需要考虑工艺误差对器件性能的影响。图8为插入损耗和$\Delta\lambda$(谐振波长与目标波长的差值)随圆孔半径的变化关系。在图8(a)中，随着布拉格反射镜中

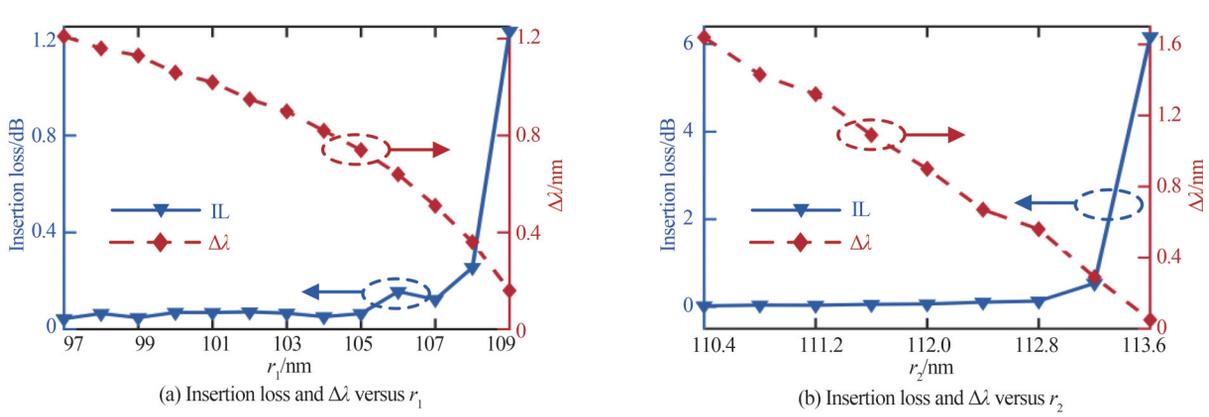

图 8　插入损耗和$\Delta\lambda$随圆孔半径的变化

Fig. 8　Insertion loss and $\Delta\lambda$ versus the radii of the holes

圆孔半径r_1的增大，$\Delta\lambda$逐渐减小，此时需要的调制电压也越小。但是当r_1大于108 nm时，调制器的插入损耗迅速增大。为了保证调制器同时具有较小的调制电压和插入损耗，r_1的变化范围为99 nm至108 nm。在图8(b)中，微腔中间两个圆孔半径r_2的变化对调制电压和插入损耗有同样的影响。在满足调制器的插入损耗小于1 dB的条件下，同时获得较小的调制电压，r_2的变化范围为111.6 nm至113.2 nm。

2.2 纳米线波导MDM器件的结构设计

纳米线波导模分复用器采用非对称定向耦合型结构，其三维结构如图9(a)所示，结构参数为：单模波导的宽度w_1=0.55 μm，单模波导与多模波导的间距g=100 nm。在相位匹配区1，多模波导的宽度w_2=1.131 μm，耦合长度L_1=24 μm。在相位匹配区2，多模波导的宽度w_3=1.716 μm，耦合长度L_2=29 μm。当波长为1 570 nm时，纳米线波导不同模式的有效折射率如图9(b)所示。当单模波导中基模的有效折射率与多模波导中高阶模的有效折射率相等时可以实现不同模式的转换。根据模式匹配原理，在相位匹配区1，可以实现TE_0模转换为TE_1模；在相位匹配区2，可以实现TE_0模转换为TE_2模。

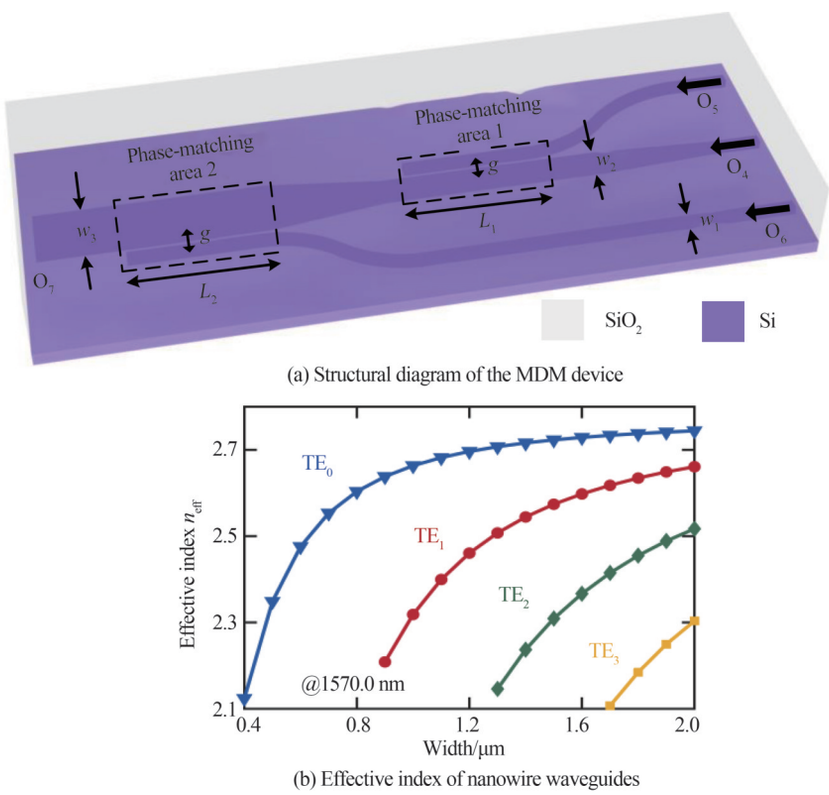

图9 三维结构图和有效折射率图

Fig. 9 Three-dimensional schematic diagram and effective index

MDM模块中不同模式的转换效率如图10所示。TE_0模光源分别从端口O_4、O_5和O_6输入，经过模式转换，在端口O_7得到TE_0模、TE_1模和TE_2模。当波长为1 570 nm时，插入损耗小于0.1 dB，信道串扰小于−26 dB。该模分复用器可以应用于1 400 nm至1 700 nm的波长范围，覆盖S、C、L、U波段。

在纳米线波导MDM器件的相位匹配区中，多模波导的宽度会影响模式转换效率。图11(a)为相位匹配区1中，多模波导宽度w_2的变化对TE_1模转换效率的影响。随着Δw_2的变化，TE_1模的插入损耗和信道串扰先减小后增大。这是因为多模波导宽度w_2的变化导致模式失配，TE_0模与TE_1模的转换效率降低。考虑插入损耗小于1 dB、信道串扰小于−20 dB的情况，多模波导宽度w_2在1.131 μm的基础上，减小10 nm至增大20 nm范围均可。图11(b)为相位匹配区2中，多模波导宽度w_3的变化对TE_2模转换效率的影响。随着Δw_3的变化，信道串扰均小于−20 dB。为了保证TE_2模的插入损耗小于1 dB，Δw_3的变化范围为−30 nm至+40 nm。

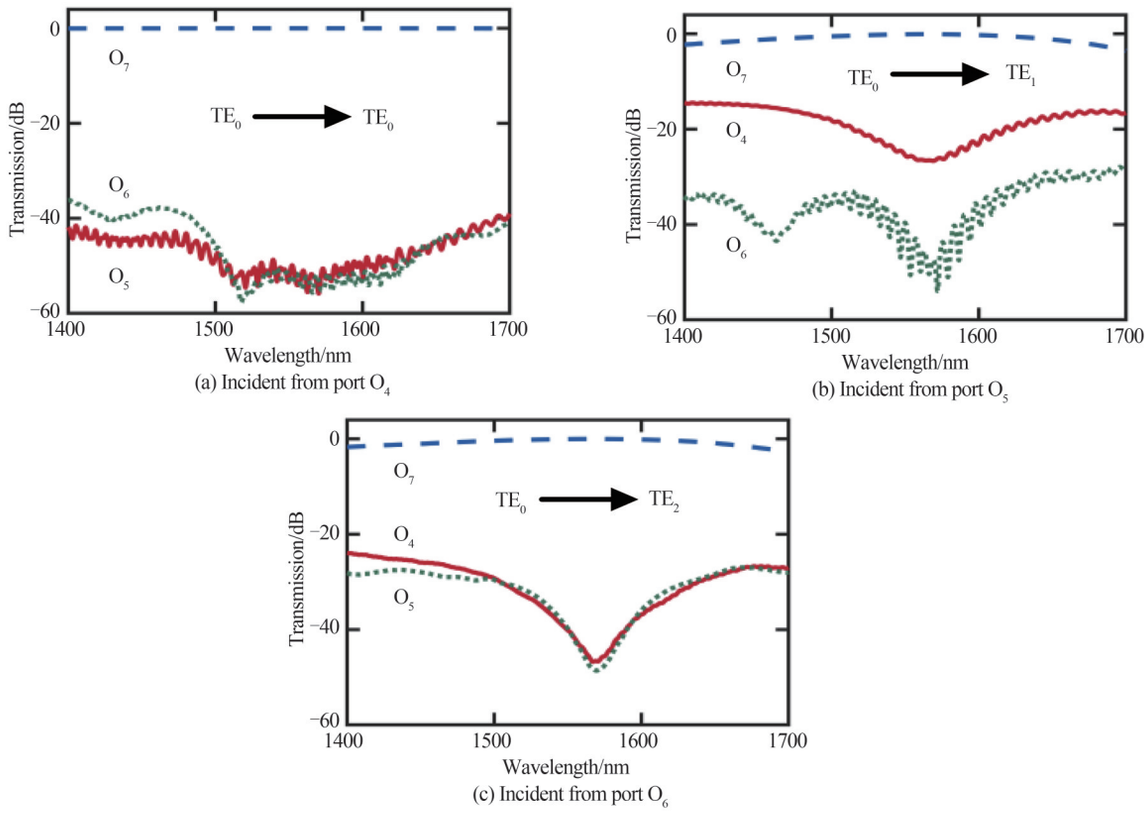

图 10　不同端口入射的透射谱

Fig. 10　Transmission spectrum incident from different ports

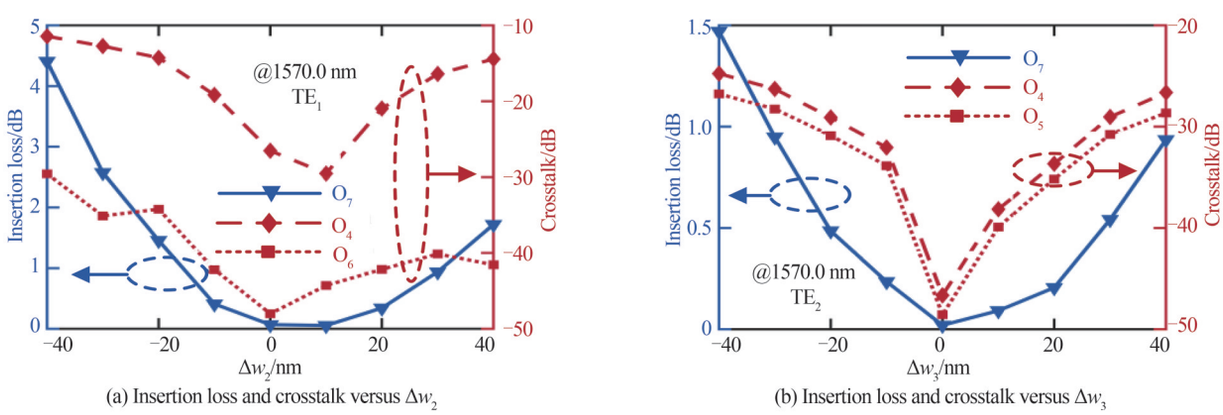

图 11　插入损耗和信道串扰随多模波宽度的变化

Fig. 11　Insertion loss and crosstalk versus the widths of the multi-mode waveguides

2.3　调制器和 MDM 集成器件的仿真分析

将三个电光调制器和一个 MDM 器件集成，构成电光调制和模分复用集成器件，其三维结构如图 4 所示。为了保证三个调制器的谐振波长均为 1 570 nm，微腔中心两个圆孔的半径需要微调。O_1端口的圆孔半径微调为 112.1 nm，O_2端口的圆孔半径微调为 112.3 nm，O_3端口的圆孔半径微调为 112.0 nm。

改变电压，调制器和 MDM 集成器件可以实现“通”“断”调制。当波长为 1 570 nm 时，该集成器件 TE_0模的透射谱如图 12(a)所示，调制器为“通”状态时，插入损耗为 0.12 dB；调制器为“断”状态时，透过率为 0.21%。因此得到 TE_0模时的消光比为 28.8 dB。该集成器件 TE_1模的透射谱如图 12(b)所示，调制器为“通”状态时，插入损耗为 0.20 dB；调制器为“断”状态时，透过率为 0.24%。因此得到 TE_1模时的消光比为 29.3 dB。同样的，该集成器件 TE_2模的透射谱如图 12(c)所示，调制器为“通”状态时，插入损耗为 0.21 dB；

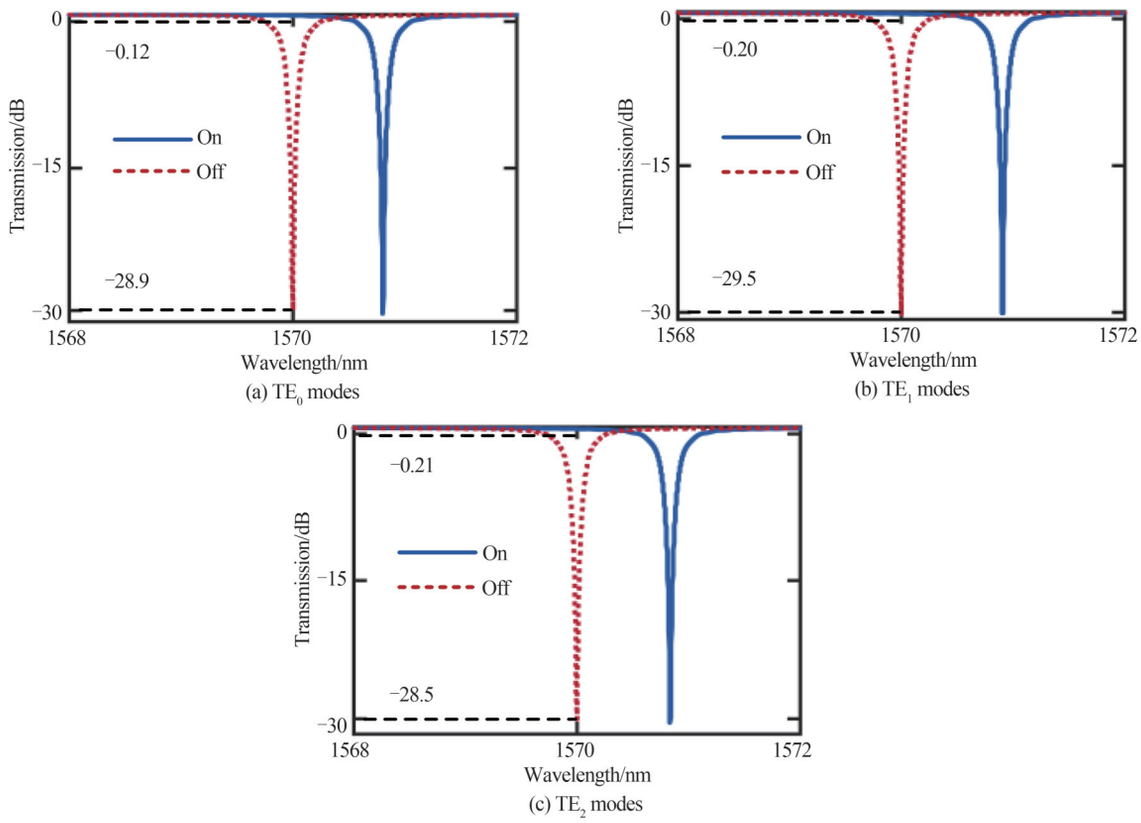

图 12 集成器件的透射谱

Fig. 12 Transmission spectrum of the integrated device

调制器为“断”状态时，透过率为0.22%。因此得到TE_2模时的消光比为28.3 dB。

经过计算，集成器件的性能参数如表1所示。可知，当波长为1 570 nm时，消光比大于28.3 dB，插入损耗小于0.21 dB，信道串扰小于−28.6 dB。插入损耗主要来源于两部分，包括调制器中的损耗(0.07 dB)和MDM器件中的损耗(0.1 dB)。

表 1 集成器件的性能参数

Table 1 Performance parameters of the integrated device

Mode	Extinction Ratio/dB	Insertion Loss/dB	Crosstalk/dB		
			O_1	O_2	O_3
TE_0	28.8	0.12	—	−45.4	−54.7
TE_1	29.3	0.20	−28.6	—	−46.5
TE_2	28.3	0.21	−48.4	−48.5	—

图13为集成器件的系统响应时间。系统响应时间为T=45 ps，由此可以得到集成器件的调制速率为44 Gbps[25-26]。

图14(a)～(f)分别为1 570 nm波长时，TE_0模、TE_1模和TE_2模的调制和模分复用过程中的稳态场分布。可以看出，调制器为“通”状态时，光波从端口O_7输出；调制器为“断”状态时，光波几乎全部被调制器的谐振腔局域，不能通过调制器。

本文提出的三信道石墨烯电光调制和模分复用集成器件与参考文献的性能对比如表2所示。

从表2中可以看出，与参考文献[5]、[7]和[27]相比，该集成器件的调制电压并不是最低，不具优势。与参考文献[17]、[18]和[27]相比，该集成器件有较大的消光比(>28.3 dB)和较小的信道串扰(<−28.6 dB)。同时，相比于表中所列对比文献，本文提出的三信道石墨烯电光调制和模分复用集成器件具有更小的插入损耗(<0.21 dB)、更大的3 dB带宽(100 GHz)和更低的能耗(0.25 pJ·bit^{-1})。

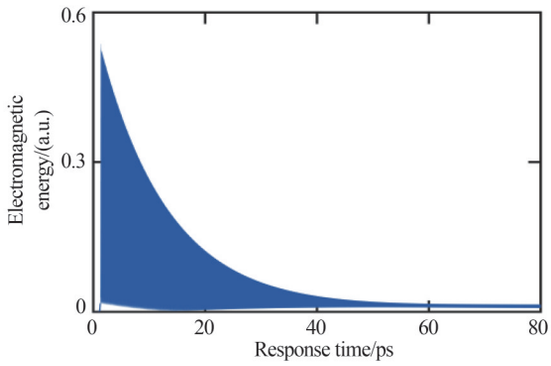

图 13　集成器件的系统响应时间

Fig. 13　System response time of the integrated device

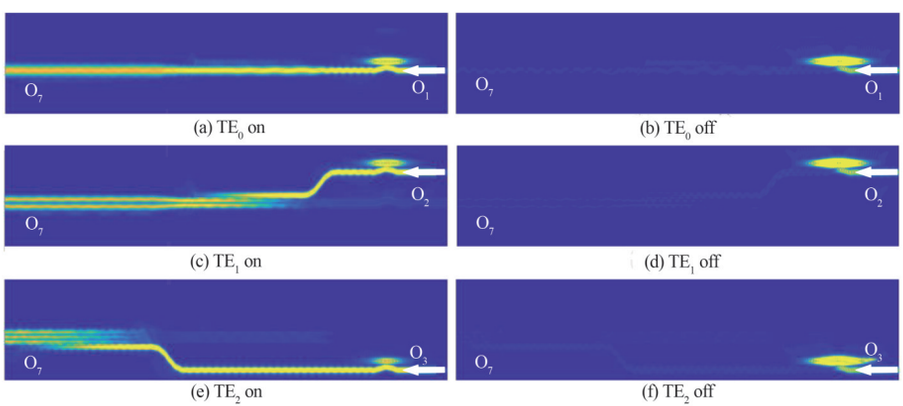

图 14　集成器件的稳态场分布

Fig. 14　Field distribution of the integrated device

表 2　不同器件的性能对比

Table 2　Comparison of reported devices

Ref.	ER/dB	IL/dB	CT/dB	3 dB/GHz	Voltage/V	MS/Gbps	E/(pJ·bit^{-1})
[3]	＞19.3	＜1.7	—	1	8.16	—	16
[4]	22	1.3	—	71	5	—	—
[5]	37	—	—	0.85	1.11	—	23.6
[7]	29	—	—	42	1.6	—	1.55
[17]	20	＜2.1	＜−19.7	—	2.5	—	—
[18]	—	＞10	＜−23.1	—	2	34	—
[19]	＞36.5	＜4.1	＜−30	—	2(3)	26(72)	—
[27]	19.73	＜0.46	＜−14.66	—	1.24	—	—
This work	＞28.3	＜0.21	＜−28.6	100	3.8	44	0.25

ER: Extinction ratio, IL: Insertion loss, CT: Channel crosstalk, MS: Modulation speed, E: Energy consumption

3　结论

提出了一种三信道石墨烯电光调制和纳米线波导模分复用集成器件。通过改变石墨烯的化学势实现调制器的“通”“断”调制。根据模式匹配原理，MDM 器件利用纳米线波导实现模式转换。仿真结果表明，该集成器件可以同时实现 TE_0、TE_1 和 TE_2 模的调制和模分复用功能。消光比大于 28.3 dB，插入损耗小于 0.21 dB，信道串扰小于 −28.6 dB，调制器的 3 dB 带宽达到 100 GHz。该集成器件可以应用于高速大容量光通信系统中。

参考文献

[1] HIRAKI T, AIHARA T, HASEBE K, et al. Heterogeneously integrated III-V/Si MOS capacitor Mach-Zehnder

modulator[J]. Nature Photonics, 2017, 11(8): 482-485.
[2] WANG Shuirou, CHEN Heming, LIU Xue, et al. An integrated device for electro-optic modulation and wavelength division multiplexing with the wavelength channel spacing of 3.2 nm[J]. Acta Photonica Sinica, 2022, 51(5): 0551312.
王水柔,陈鹤鸣,刘雪,等. 波长间隔为3.2 nm的电光调制和波分复用集成器件研究[J]. 光子学报, 2022, 51(5): 0551312.
[3] WANG Jiaqi, ZHANG Xinying, CHEN Yuzhi, et al. Design of a graphene-based silicon nitride multimode waveguide-integrated electro-optic modulator[J]. Optics Communications, 2021, 481: 126531.
[4] REZAEI M H, SHIRI M. High-performance tunable resonant electro-optical modulator based on suspended graphene waveguides[J]. Optics Express, 2021, 29(11): 16299-16311.
[5] LIAN Tianhang, YANG Kaidi, SUN Shijie, et al. Polarization-independent electro-absorption optical modulator based on trapezoid polymer-graphene waveguide[J]. Optics & Laser Technology, 2022, 149: 107815.
[6] KIM S, MENABDE S G, COX J D, et al. Ultracompact electro-optic waveguide modulator based on a graphene-covered λ/1000 plasmonic nanogap[J]. Optics Express, 2021, 29(9): 13852-13863.
[7] LIAN Tianhang, YANG Kaidi, WANG Xibin, et al. Electro-absorption optical modulator based on graphene-buried polymer waveguides[J]. IEEE Photonics Journal, 2020, 12(4): 1-10.
[8] SORIANELLO V, MIDRIO M, ROMAGNOLI M. Design optimization of single and double layer Graphene phase modulators in SOI[J]. Optics Express, 2015, 23(5): 6478-6490.
[9] CHEN Kaixuan, LIU Liu, HE Sailing. Mode division multiplexing based on supermodes in densely packed uniform waveguide array (DPUWA)[J]. IEEE Photonics Journal, 2020, 12(2): 1-10.
[10] HAN Xu, XIAO Huifu, LIU Zilong, et al. Reconfigurable on-chip mode exchange for mode-division multiplexing optical networks[J]. Journal of Lightwave Technology, 2019, 37(3): 1008-1013.
[11] ZHANG G, MOJAVER H R, DAS A, et al. Mode insensitive switch for on-chip interconnect mode division multiplexing systems[J]. Optics Letters, 2020, 45(4): 811-814.
[12] GOSTIMIROVIC D, YE W N. Compact silicon-photonic mode-division (de) multiplexer using waveguide-wrapped microdisk resonators[J]. Optics Letters, 2021, 46(2): 388-391.
[13] LIU Yingjie, WANG Zi, LIU Yilin, et al. Ultra-compact mode-division multiplexed photonic integrated circuit for dual polarizations[J]. Journal of Lightwave Technology, 2021, 39(18): 5925-5932.
[14] DING Hongjie, LIU Peng, LIU Yong, et al. Research on designing approaches for device and integration of photonic integrated interferometric detecting system[J]. Acta Photonica Sinica, 2021, 50(5): 0513001.
丁红杰,刘鹏,刘勇,等. 光子集成干涉探测系统关键器件和集成化设计方法研究[J]. 光子学报, 2021, 50(5): 0513001.
[15] YUE Gongcheng, XING Zhengkun, HU Haofeng, et al. Graphene-based dual-mode modulators[J]. Optics Express, 2020, 28(12): 18456-18471.
[16] LIU Xue, CHEN Heming, HU Yuchen. An integrated device for photonic crystal electro-optic modulation and coarse wavelength division multiplexing[J]. Chinese Journal of Lasers, 2021, 48(3): 0306002.
刘雪,陈鹤鸣,胡宇宸. 光子晶体电光调制和粗波分复用集成器件研究[J]. 中国激光, 2021, 48(3): 0306002.
[17] JIA Hao, FU Xin, ZHOU Ting, et al. Mode-selective modulation by silicon microring resonators and mode multiplexers for on-chip optical interconnect[J]. Optics Express, 2019, 27(3): 2915-2925.
[18] WU Xinru, HUANG Chaoran, XU Ke, et al. 3×104 Gb/s single-λ interconnect of mode-division multiplexed network with a multicore fiber[J]. Journal of Lightwave Technology, 2018, 36(2): 318-324.
[19] CHEN Guanyu, YU Yu, ZHANG Xinliang. Monolithically mode division multiplexing photonic integrated circuit for large-capacity optical interconnection[J]. Optics Letters, 2016, 41(15): 3543-3546.
[20] REN Hongliang, JIANG Chun, HU Weisheng, et al. Photonic crystal channel drop filter with a wavelength-selective reflection micro-cavity[J]. Optics Express, 2006, 14(6): 2446-2458.
[21] JOANNOPOULOS J D, JOHNSON S G, WINN J N, et al. Photonic crystals: molding the flow of light[M]. Princeton University Press, 2008: 198-203.
[22] PAN Wanle, CHEN Heming, HU Yuchen. Integrated device for graphene electro-optic modulation and one-dimensional photonic crystal nanobeam cavity wavelength division multiplexing[J]. Applied Physics B, 2022, 128 (5): 95.
[23] DU Wei, LI Erping, HAO Ran. Tunability analysis of a graphene-embedded ring modulator[J]. IEEE Photonics Technology Letters, 2014, 26(20): 2008-2011.
[24] QIU C, GAO W, VAJTAI R, et al. Efficient modulation of 1.55 μm radiation with gated graphene on a silicon micro-ring resonator[J]. Nano Letters, 2014, 14(12): 6811-6815.
[25] CHEN Heming, SU Jian, WANG Jingli, et al. Optically-controlled high-speed terahertz wave modulator based on nonlinear photonic crystals[J]. Optics Express, 2011, 19(4): 3599-3603.
[26] MALEVICH Y, ERGOKTAS M S, BAKAN G, et al. Video-speed graphene modulator arrays for terahertz imaging

applications[J]. ACS Photonics, 2020, 7(9): 2374-2380.
[27] XIANG Tong, CHEN Heming, HU Yuchen. Silicon-based integrated device for electro-optic modulation assembly with mode-division multiplexing[J]. Chinese Journal of Lasers, 2021, 48(11): 1106001.
项彤,陈鹤鸣,胡宇宸. 硅基电光调制与模分复用集成器件[J]. 中国激光, 2021, 48(11): 1106001.

Three-channel Integrated Device for Graphene Electro-optic Modulation and Mode Division Multiplexing

PAN Wanle[1], CHEN Heming[2], HU Yuchen[1]
(1 *College of Electronic and Optical Engineering, Nanjing University of Posts and Telecommunications, Nanjing* 210023, *China*)
(2 *Bell Honors School, Nanjing University of Posts and Telecommunications, Nanjing* 210023, *China*)

Abstract: In the Internet era, the demand for transmission speed and transmission capacity of optical communication systems has increased significantly. Electro-optic modulators for optical communication systems are developing towards high speeds. Traditional silicon-based electro-optic modulators have a slow response speed. Graphene has excellent optical and electrical properties and is compatible with Complementary Metal Oxide Semiconductor (CMOS) processes. Combining graphene with silicon materials can improve the response speed of electro-optic modulators. At the same time, wide bandwidth, high extinction ratio, low insertion loss, and low energy consumption are the development trends of graphene electro-optic modulators. On the other hand, to meet the needs of optical communication systems, multiplexing technologies such as mode division multiplexing are used to increase the communication capacity. The research on a single-function optical communication device has gradually matured, and the combination of different devices to form an integrated device has become a research hotspot in recent years. The combination of electro-optic modulation and mode division multiplexing technology can improve the transmission speed and transmission capacity of optical communication systems. With the continuous advancement of science and technology, optical interconnection has attracted widespread attention due to its advantages of high speed, wide bandwidth and large capacity, and various integrated devices have emerged as the times require. Among them, the integrated device for electro-optic modulation and mode division multiplexing has shortcomings such as small transmission capacity and low transmission speed. Meanwhile, different devices are difficult to integrate due to differences in materials and structures.

A three-channel integrated device for graphene electro-optic modulation and mode division multiplexing is proposed, which consists of a one-dimensional photonic crystal nanobeam cavity electro-optic modulation module covered by a single-layer graphene and nanowire waveguides mode division multiplexing module. The electro-optic modulator is composed of a one-dimensional photonic crystal nanobeam cavity, a nanowire waveguide, and a silicon plate. Combining the curved waveguide with the straight waveguide improves the coupling efficiency of the one-dimensional photonic crystal nanobeam cavity and the nanowire waveguides. A layer of Al_2O_3 is covered on top of the silicon plate and the one-dimensional photonic crystal nanobeam cavity, and a single-layer graphene is added on top of the Al_2O_3. The electrodes on graphene serve as anodes, and the electrodes on silicon plates serve as cathodes. Applying a voltage changes the chemical potential of graphene, enabling modulation of specific wavelengths. According to the principle of mode matching, the mode division multiplexer adopts an asymmetric directional coupling nanowire waveguides structure. In the phase matching region, the fundamental modes in the single-mode waveguide are converted into the higher-order modes in the multi-mode waveguide, realizing the conversion of different modes. The TE_0 modes are output from the same port in the form of TE_0 modes, TE_1 modes and TE_2 modes through the graphene electro-optic modulator and mode division multiplexer, achieving the functions of electro-optic modulation and mode division multiplexing.

The performance parameters of the three-channel integrated device for graphene electro-optic modulation and mode division multiplexing are analyzed using the three-dimensional finite-difference time-

domain method. During the production and preparation of the devices, the influence of process errors on the performance of the devices needs to be considered. Therefore, important structural parameters of the graphene electro-optic modulator and nanowire waveguides mode division multiplexer are selected for tolerance analysis, respectively. At the wavelength of 1 570 nm, when the voltage is 0 V, the incident light is not coupled with the one-dimensional photonic crystal nanobeam cavity and can be transmitted along the waveguide. The modulator is in the on-state. When the voltage is 3.8 V, the chemical potential of graphene changes, resulting in a change in the equivalent refractive index of the material. Therefore, the resonance wavelength of the one-dimensional photonic crystal nanobeam cavity is shifted to match the target wavelength (1 570 nm), and the incident light is coupled into the microcavity, realizing the off-state of the modulator. The insertion loss is 0.07 dB, the extinction ratio is 22.5 dB, and the 3 dB bandwidth is about 100 GHz. The modulated incident light enters the mode division multiplexer. In the phase matching region, the effective index of the single-mode waveguide and the multi-mode waveguide is equal, and the TE_0 modes are converted into TE_1 modes and TE_2 modes. The insertion loss is less than 0.1 dB, and the channel crosstalk is less than −26 dB. The TE_0 modes input from the three ports are output from the same port in different modes.

In conclusion, a three-channel integrated device for graphene electro-optic modulation and mode division multiplexing is proposed. The integrated device can realize modulation and mode division multiplexing of TE_0 modes, TE_1 modes, and TE_2 modes at the same time. The simulation results using the three-dimensional finite-difference time-domain method show that when the wavelength is 1 570 nm, the extinction ratio of the integrated device is greater than 28.3 dB, the insertion loss is less than 0.21 dB, the channel crosstalk is less than −28.6 dB, and the 3 dB bandwidth of the modulator reaches 100 GHz. The integrated device has excellent performance and has important application value in high-capacity optical communication systems.

Key words: Graphene; Nanowire waveguides; Electro-optic modulation; Mode division multiplexing; Silicon-based optoelectronics integration

OCIS Codes: 230.2090; 230.7370; 060.4230

Foundation item: National Natural Science Foundation of China (No. 61571237), Natural Science Foundation of Jiangsu Province (No. BK20151509), Postgraduate Research & Practice Innovation Program of Jiangsu Province (Nos. KYCX20_0740, KYCX20_0769)